PROCEEDINGS OF SPIE

SPIEDigitalLibrary.org/conference-proceedings-of-spie

Reflective coatings for the future x-ray mirror substrates

Hideyuki Mori, Takashi Okajima, William W. Zhang, Kai-Wing Chan, Richard Koenecke, et al.

Hideyuki Mori, Takashi Okajima, William W. Zhang, Kai-Wing Chan, Richard Koenecke, James R. Mazzarella, Ai Numata, Lawrence G. Olsen, Raul E. Riveros, Mihoko Yukita, "Reflective coatings for the future x-ray mirror substrates," Proc. SPIE 10699, Space Telescopes and Instrumentation 2018: Ultraviolet to Gamma Ray, 1069941 (6 July 2018); doi: 10.1117/12.2313469

SPIE.

Event: SPIE Astronomical Telescopes + Instrumentation, 2018, Austin, Texas, United States

Reflective Coatings for the Future X-ray Mirror Substrates

Hideyuki Mori[a,b,c], Takashi Okajima[c], William W. Zhang[c], Kai-Wing Chan[a,b,c], Richard Koenecke[c], James R. Mazzarella[c], Ai Numata[c], Lawrence G. Olsen[c], Raul E. Riveros[c], and Mihoko Yukita[c,d]

[a]Center for Research and Exploration in Space Science and Technology (CRESST II), Greenbelt, MD 20771, USA
[b]Department of Physics, University of Maryland, Baltimore County, 1000 Hilltop Circle, Baltimore, MD 21250, USA
[c]X-ray Astrophysics Laboratory, NASA's Goddard Space Flight Center, Greenbelt, MD 20771, USA
[d]Johns Hopkins University, Homewood Campus, Baltimore, MD 21218, USA

ABSTRACT

We present the development of the reflective coating by magnetron sputtering deposition onto precisely-fabricated thin X-ray mirrors. Our goal is to remove distortion induced by the coating and then keep their surface profiles. We first addressed the uniform coating to minimize the distortion by introducing a mask to control the spatial distribution of the coating thickness. The uniformity was finally achieved within ±1%. We next tried a platinum single-layer coating on a glass substrate with a dimension of 200 mm × 125 mm. The distortion caused by the frontside coating with a thickness of 320 Å was found to be at most ∼ 1 μm, smaller than the previous results obtained from the non-uniform coating. We then carried out the platinum coating with the same amount of the thickness on the backside surface of the glass substrate. The surface profile of the glass substrate was fully recovered, indicating that the residual stress was successfully balanced by the backside coating. Furthermore, we tried to an iridium single-layer coating with a thickness of 150 Åon the silicon mirrors. The frontside coating caused the degradation of the imaging quality by 7.5 arcsec in half-power width. However, the backside coating with the same amount of the thickness reduced this degradation to be 3.4 arcsec. Finally, an additional backside coating with a thickness of 100 Å and the annealing to relax the residual stress were found to eliminate the distortion completely; the final degradation of the imaging quality was only 0.4 arcsec.

Keywords: X-ray mirrors, reflective coating, residual stress, DC magnetron sputtering

1. INTRODUCTION

For the next-generation X-ray telescopes, an X-ray mirror with high throughput and supreme angular resolution is a strong demand since it allows us to obtain high X-ray sensitivity enough to resolve discrete faint X-ray sources and to reveal fine spatial structures of diffuse X-ray emission, such as supernova remnants or clusters of galaxies. The fabrication of thin and high-precision X-ray mirror substrates is one of the key technologies to be addressed towards the achievement of this goal. Some new approaches have been developed so far, such as silicon meta shells,[1,2] full-shell mirrors,[3] adjustable mirrors,[4] and silicon pore optics.[5,6]

Besides of the fabrication of highly-precised thin mirror shells, the reflective coating is necessary to enhance the X-ray reflectivity at higher X-ray energies. However, it is well known that the residual stress of the coating layer causes severe distortion of the thin shells. To achieve an imaging capability at the sub-arcsecond level, the removal of the distortion is also an important issue to be resolved.[7] There are several techniques to address this issue. One of them is a selection of the coating material which has less residual stress to minimize the distortion. Bi-layer coating is another solution; for example, iridium/chromium bi-layer can reduce the residual stress since the compressive stress of the iridium can be canceled out by the tensile stress of the chromium.[8]

Further author information: (Send correspondence to H.M.)
H.M.: E-mail: hideyuki.mori@nasa.gov, Telephone: 1 301 614 6013

Space Telescopes and Instrumentation 2018: Ultraviolet to Gamma Ray, edited by Jan-Willem A. den Herder, Shouleh Nikzad, Kazuhiro Nakazawa, Proc. of SPIE Vol. 10699, 1069941 · © 2018 SPIE
CCC code: 0277-786X/18/$18 · doi: 10.1117/12.2313469

We present here the development of the reflective coating technique to minimize the distortion by balancing the residual stress with the backside coating. We first explain the equipments we use for the reflective coating and its evaluation in Sec. 2. The uniformity of the coating thickness we first addressed is described in Sec. 3. The results of the frontside and the backside coatings on the glass substrates and the silicon mirrors are also explained in this section. The summary of our study and the future prospect is given in Sec. 4.

2. EQUIPMENTS FOR THE COATING STUDY

2.1 Reflective Coating Chamber

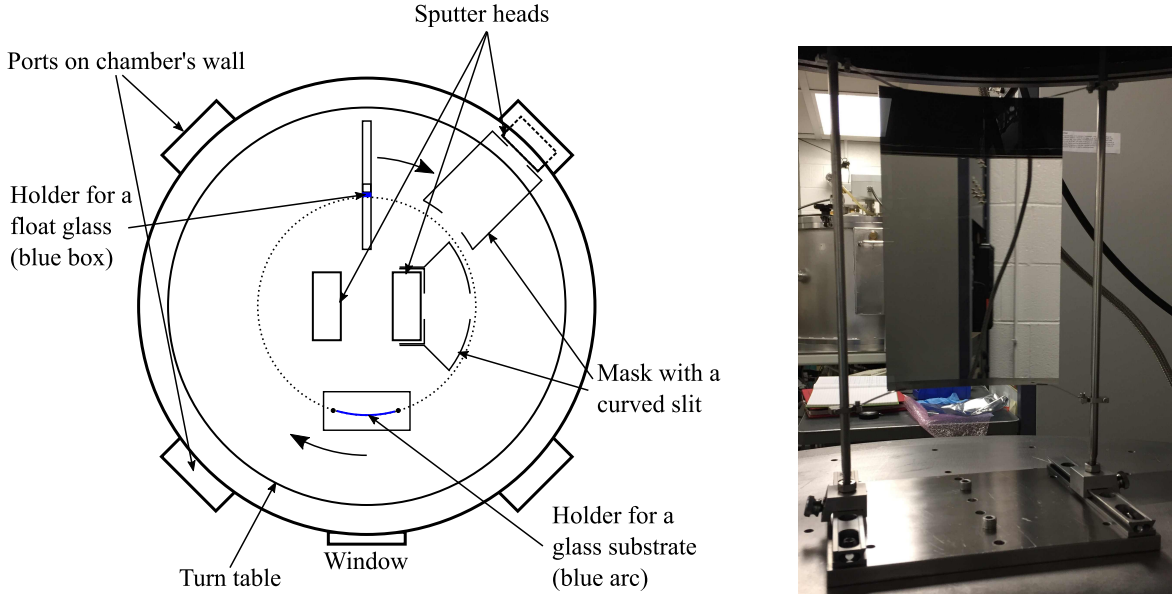

Figure 1. Schematic top view of the coating chamber (left) and a picture of a glass substrate and its holder after the frontside coating (right).

The left panel of Fig. 1 shows a schematic top view of our coating chamber. The chamber has a cylindrical shape, consisting of a base plate, a wall, and a lid. We have a total of 6 ports to mount sputtering heads. The coating materials with a dimension of 203.2 mm × 50.8 mm (8" × 2") are installed in these sputtering heads, and then are deposited on substrates by the DC magnetron sputtering method. As shown in the left panel of Fig. 1, two sputtering heads are placed at the center of the chamber, and the others are done in the chamber's wall. In the current configuration, we use two sputtering heads for the frontside coating, and one head in the wall for the backside coating. We can change the reflective materials such as platinum (Pt) or iridium (Ir), depending on the purposes of our study. For the multilayer coating, we also use a carbon (C) target. Not only a magnet but also a water-flow tube are installed in each sputtering head to cool down the materials during the coating.

The inside of the chamber is pumped down by a rotary and a cryogenic pumps so that the vacuum pressure could be decreased to $\sim 4 \times 10^{-6}$ Torr. We use argon (Ar) gas as sputtering particles that react with the coating material. The flow speed and the pressure of the Ar gas is set to be 80 sccm and 4×10^{-3} Torr, respectively. In order to stabilize the sputtering rate during the coating, we use the DC power supply boxes (MDX-1.5K/DCG-100A OPTIMA) in the current regulation mode. The system is automated and then is controlled remotely from the LabVIEW panel implemented in the desktop PC.

The chamber also has a turn table with a radius of 431.8 mm (17"). By setting up a sample on the table and then rotating it, we can switch the deposition of the reflective materials selectively. We made sample holders both for Borofloat/Soda lime glass and glass/silicon substrates. The surface position of the samples was set to be 198 mm in radius from the center of the turn table. Furthermore, we also made masks attached on the sputtering heads to regulate the direction of the sputtered materials, as shown in the left panel of Fig. 1. Each mask has

two slits; while the one near the sputtering head has a rectangular shape with a width of 30 mm, the shape of the other one looks like a concave lens. The design of the masks is explained later in Sec. 3. The thickness of the reflective layer is determined by an exposure time to the sputtered particles. Thus, the thickness can be controlled by adjusting a rotational speed of the turn table. We also explain the relation between the thickness and the rotational speed in Sec. 3. The right panel of Fig. 1 shows a picture of a glass substrate installed on the holder after the frontside coating.

2.2 X-Ray Reflectometer

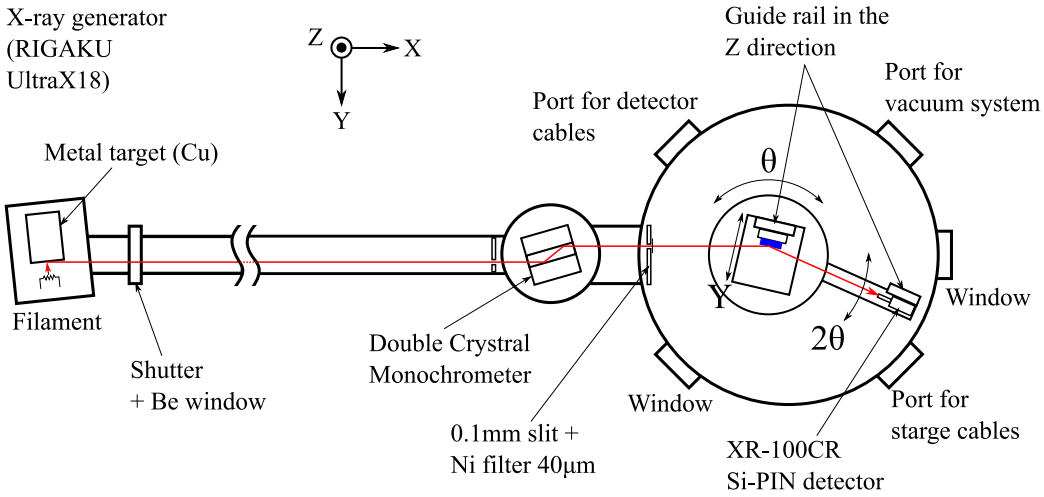

Figure 2. Schematic top view of the X-ray reflectometer. Thermoelectrons emitted from a filament and the resultant X-rays are shown by red arrows. A blue box represents a coated sample.

The properties of the coated sample, such as the thickness and the surface roughness of the reflective layer, were evaluated by the X-ray reflectivity. Fig. 2 shows a schematic top view of our X-ray reflectometer, which is used to measure the dependence of the X-ray reflectivity on the incident angles. The X-ray reflectometer consists of a rotating anode X-ray generator, RIGAKU UltraX18, and a chamber that accommodates the coated sample and an X-ray detector. The X-ray generator emits the continuum and the characteristic X-rays, depending on the metal target we use. For the evaluation of the sample, we used the Cu-Kα emission line at 8.04 keV. We used a filament with a size of 0.3 mm $\times$ 3 mm. The spot size of the X-ray beam was $\sim$ 0.3 mm $\times$ 0.3 mm on the rotating target. A beryllium (Be) window and a shutter are equipped in the generator.

Here, we define the coordinates so that the +X axis should be parallel to the direction of the incident X-ray beam and the +Z axis should be the vertical upward direction. The X-ray generator and the chamber are connected by a duct. The distance between the generator and the entrance of the chamber is $\sim$ 3 m. The double crystal monochrometer (DCM) is installed in front of the entrance of the chamber in order to monochromatize the incident X-rays using the Bragg condition. The DCM direction is optimized for the Cu-Kα line. In addition, there are two slits to make the beam width narrow (0.1 mm) in the duct and at the entrance of the chamber, as shown in Fig. 2. We also attach a nickel (Ni) filter with a thickness of 40 μm on the slit at the chamber's entrance to reduce the residual continuum X-rays.

The coated sample is installed in a specific holder. The holder is mounted on a vertical guide rail, which allows us to adjust the sample height to the incident beam position. The guide rail is attached on a translation stage that moves in the Y direction. The translation stage is mounted on a goniometer, which can rotate the sample. During the sample alignment, we adjust the rotational center of the sample to that of the goniometer. As a detector, we used a Si-PIN detector, XR-100CR (Amptek Inc.). The detector is also mounted on another vertical guide rail. This rail is attached on a horizontal guide rail, which is mounted on another goniometer. While the sample is rotated by θ, the detector is done by 2θ, and then we can measure the intensity of the

reflected X-ray beam. The inside of the chamber is pumped by a rotary pump during the measurement; a typical vacuum pressure is below 5×10^{-2} Torr.

3. RESULTS

3.1 Control of the Coating Thickness

We first made the mask placed in front of the reflective material (hereafter target) to control the spatial distribution of the coating thickness in the vertical direction (see Fig. 1). For the uniform coating in this direction, we tuned the shape of the slit on the near side of the rotated samples. The gap between the sample and this slit was set to ~ 5 mm to avoid that the sputtered particles are deposited diagonally to the sample as much as possible. We first performed the Pt single-layer coating using a rectangular slit with a width of 30 mm. Four pieces of float glass (each piece has a dimension of 70 mm $\times$ 30 mm $\times$ 3 mm) were used so that the sample could cover ~ 200 mm height of the Pt target. After the coating, we measured the spatial distribution of the coating thicknesses in the vertical direction. The result is shown in the left panel of Fig. 3. The coating thickness became thinner by $\sim 50\%$ at the positions, corresponding to the edges of the Pt target. Thus, we decreased the slit width so that the thickness should be 180 μm uniformly over the range of 200 mm as follows: $w(z) = 180/d(z) \times 30$ mm. Here $w(z)$ and $d(z)$ represent the slit width and the coating thickness at a given vertical position. After some iterations, we achieved the uniformity of the coating thicknesses of $\pm 1\%$, as shown in the right panel of Fig. 3. The slit widths in the final design were 14.46 mm at $z = 0$ mm, 24.22 mm at $z = -100$ mm, and 25.05 mm at $z = +100$ mm. The shape of the slit depends on the magnetic fields applied on each sputtering head. Thus, we repeated the same procedure to determine the slit widths of the mask for the sputter head installed in the chamber's wall. The uniformity of the backside coating is also shown in the right panel of Fig. 3.

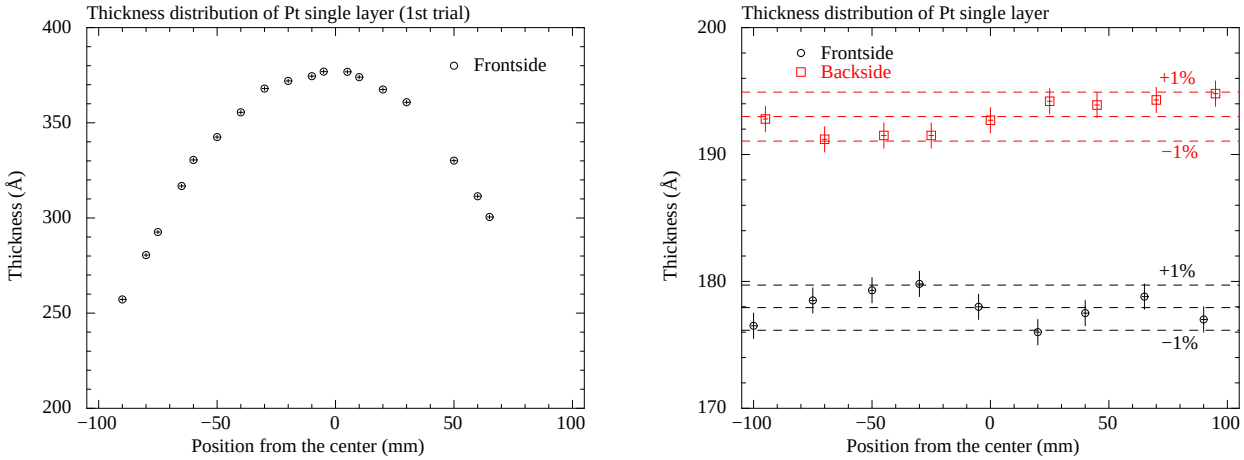

Figure 3. Spatial distribution of the thicknesses of the Pt single layer, using a rectangular slit (left) and a curved slit (right). In the right panel, we show the spatial distribution both for the frontside and backside coatings.

After establishing the uniformity, we next investigated the relation between the rotational speed (v) of the turn table and the coating thickness (d). Fig. 4 shows the resultant relation. Since the path length along which the sample is exposed to the sputtered particles is 14.46 mm at the center of the target, we can convert the rotational speed to the exposure time (t) by $t = 14.46/v$. We fitted the data points indicated with the red open circles in Fig. 4 by a linear function. The best-fit function was $d = (6.05 \pm 0.02) \times t + (0.06 \pm 1.12)$, indicating that the linearity of the coating thickness was assured up to ~ 400 Å. We note that the resolution of the rotational speed is limited to be 0.042 degree s^{-1}, which is determined by the specification of the step motor driver. We installed a gear box to mitigate this limit; the current resolution is ~ 0.002 degree s^{-1}. However, due to this limitation, the thickness above 400 Å cannot be controlled continuously. The blue open squares in Fig. 4 are examples of the deviation due to the resolution limit of the rotational speed. We also note that the reproducibility of the coating was $\lesssim 1\%$ as indicated by two red open circles with a thickness of 400 Å.

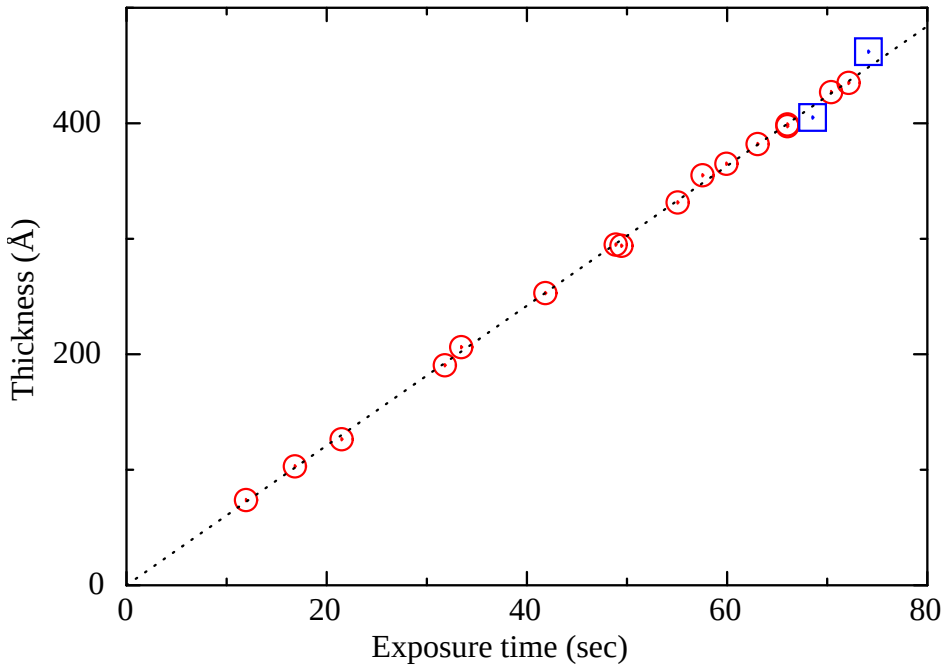

Figure 4. Relation between the exposure time to the sputtered particles and the coating thickness. A dotted line indicates the best-fit linear function derived from red open circles. The blue open squares represent the thicknesses that we cannot control only by the rotational speed.

3.2 Frontside and backside coatings on the glass and silicon mirrors

We performed the Pt single-layer coating on the surface of the thin glass substrate. The height and width of the substrate were 200 mm and 125 mm, respectively. The thickness of the substrate was 0.4 mm. The width corresponds to the azimuthal angle of 30 degree. We tried the coating with two different thickness: 150 and 320 Å. In order to investigate distortion induced by the reflective coating, we measured the surface profile before and after the coating, using the optical interferometer, FizCam 2000 (4D Technology Corp.). Fig. 5 shows the color maps of the surface profiles of the glass substrate. The middle panel of Fig. 5 indicates the surface profile after the frontside coating with a thickness of 320 Å.

Furthermore, we extracted the axial profiles at the azimuthal angles of 0 (center), and ±10 degree (edges), as shown in Fig. 6. The axial profiles clearly show that the glass substrate was distorted by the reflective coating. We note that the directions of the distortion were different between the center and the edges of the glass substrate. The axial profiles at the edges were changed by ~ 1 μm in the convex shape. On the other hand, the substrate was bent by ~ 0.5 μm in the concave shape at the center. It is also noteworthy that the amount of the distortion was at most ~ 1 μm, which was smaller than the previous studies[7,8] where the distribution of the coating thicknesses was not uniform.

We next performed the Pt single-layer coating on the backside surface of the glass substrate. The coating thickness was set to the same as that of the frontside coating. However, the actual thickness was found to be slightly larger (by $\sim 15\%$) than our expectation from the X-ray reflectivity measurement. The resultant surface profile of the glass substrate is shown in the right panel of Fig. 5. The axial profiles after the backside coating are also shown with blue curves in Fig. 6. The color map and the axial profiles after the backside coating indicate that the surface profile was fully recovered to that before the coatings. We demonstrated that the residual stress induced by the reflective coating can be balanced by performing the backside coating.

After the achievement of the stress balancing for the glass substrate, we also performed the coating of two

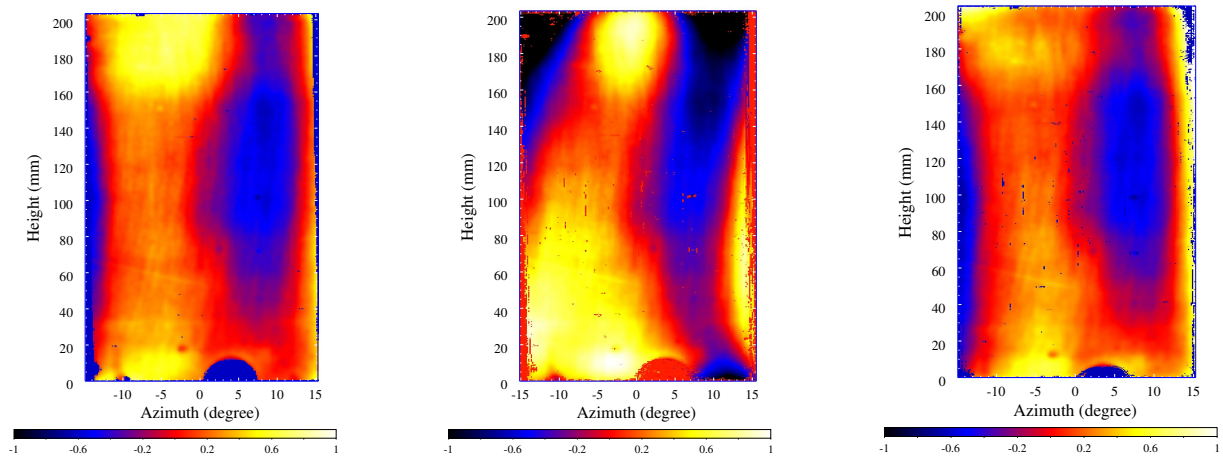

Figure 5. Color maps of the surface profiles of the glass substrate before the coating (left), after the frontside coating (middle), and after the backside coating (right). We normalized the average of the surface profiles to be zero. The color scales in the bottom are in unit of μm.

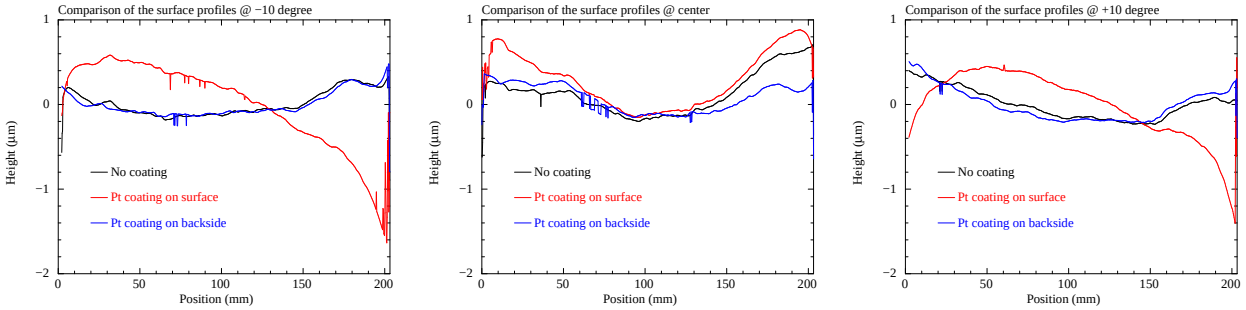

Figure 6. Axial profiles of the glass substrate before the coating (black curve), after the frontside coating (red curve), and after the backside coating (blue curve). These profiles were extracted from the 2-dimensional surface profiles at azimuthal angles of −10 (left), +0 (middle), and +10 (right) degrees.

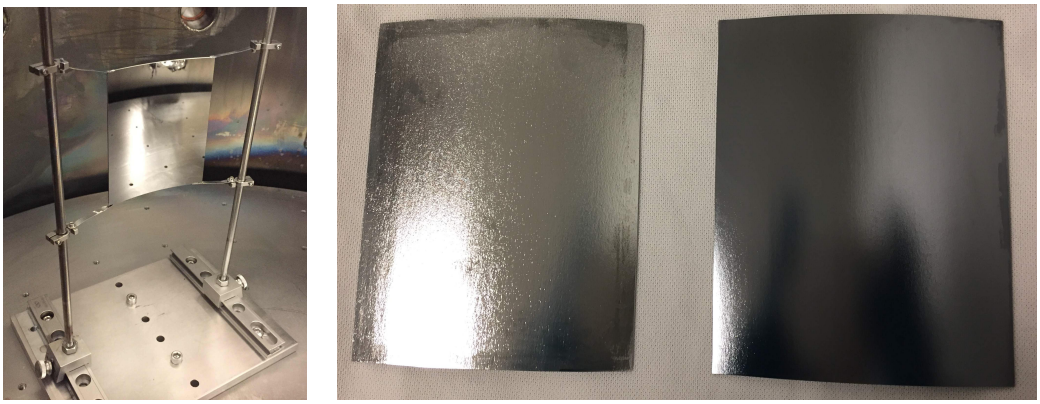

Figure 7. Pictures of the silicon mirrors with its holder (left) and their backside surfaces (right).

silicon mirrors,[2] as shown in the left panel of Fig. 7. The thickness of these silicon mirrors were 0.7 mm and 0.5 mm. We first performed the Ir coating with a thickness of 146 Å on the frontside surface of the silicon mirror. In addition, to balance the residual stress of this Ir layer, we next carried out the backside coating with the same thickness of 146 Å. The history of the imaging quality of the silicon mirrors are summarized in Table 1. Here we use the half-power width (HPW) to evaluate the imaging quality of the mirrors; the difference in the HPW from the silicon mirrors without any coatings are shown in Table 1. We found that the backside Ir coating with the same amount of the thickness cannot balance the residual stress completely. Different from the glass substrates, the backside surface of the silicon mirrors is quite rough compared with the polished frontside surface, as is shown in the right panel of Fig. 7. Thus, the residual stress in the backside Ir layer should not fully work to mitigate the distortion. However, the backside coating was still effective, and then reduced the change the HPW to be 3.4 arcsec. We also tried the annealing of the silicon mirrors to reduce the residual stress, which resulted in the improvement of the HPW by 1.4 arcsec. Finally, we performed an additional backside coating with a thickness of 100 Å. The change of the HPW at this stage was 0.4 arcsec, indicating again that the backside coating is quite effective even for the silicon mirrors to remove the distortion by the single-layer coating.

Table 1. History of the imaging quality of the silicon mirrors.

	Frontside coating	Backside coating	Annealing	Additional Backside coating
ΔHPW (arcsec)	7.5	3.4	2.0	0.4

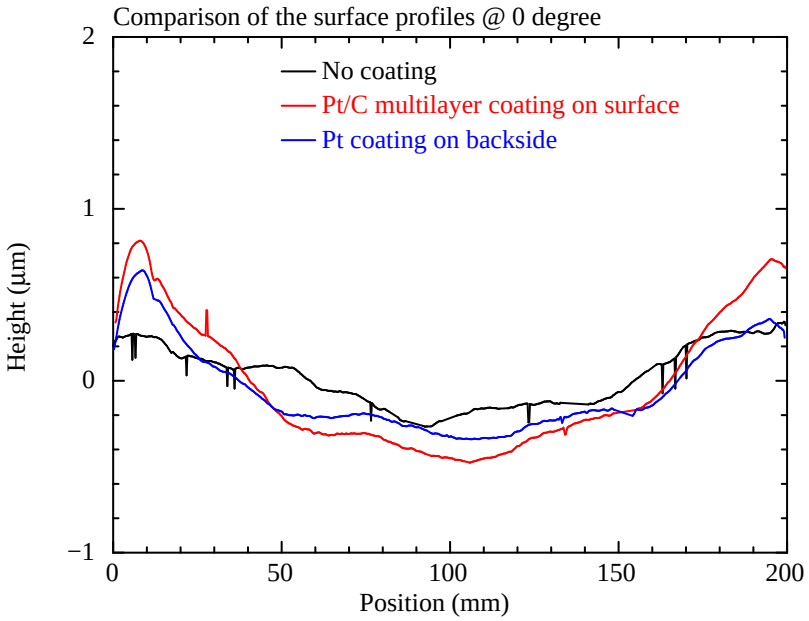

Figure 8. Axial profile of the glass substrate before the coating (black curve), after the Pt/C multilayer coating on the frontside surface (red curve), and after the Pt single-layer coating on the backside surface (blue curve).

As a next step, we investigated whether the stress balancing by the backside coating can be applied to the multilayer. Then, we carried out the Pt/C multilayer coating on the frontside surface of a glass substrate. The parameters of the Pt/C multilayer we adopted was the same as Group 8 used in the ASTRO-H HXT.[9,10] The total number of the Pt/C pairs is 138; the total thicknesses of the Pt and C are $\sim$ 1100 Å and $\sim$ 1700 Å, respectively. The 2-dimensional surface profiles before and after the coating were measured in the same manner described above. The axial profile, corresponding to the center in the azimuthal direction, is shown in Fig. 8. The axial profile was found to be changed by ~ 0.8 μm in the concaved shape. To mitigate the residual stress induced by this multilayer, we carried out the backside coating; we here deposited the Pt single layer on the

backside surface. We first tried the coating with a thickness of 400 Å, and then gradually increased the thickness to investigate the change of the distortion. However, the axial profile was not recovered by the backside coating of the Pt single layer even with a thickness of 1100 Å, as shown in Fig. 8. This result indicates that the distribution of the residual stress is quite different between the single layer and multilayer. The detailed understanding of the residual stress induced by the multilayer coating should be necessary to balance the stress by the backside coating.

4. SUMMARY

We addressed the distortion-free reflective coating on the thin X-ray mirrors by introducing the backside coating to balance the residual stress in the coating layer. First, we focused on the control of the quality of the coating layer, in particular the spatial distribution of the coating thickness. Since our coating chamber has a turn table to rotate the sample, the reflective materials can be deposited axisymmetrically on the sample's surface. To regulate the direction of the sputtered materials, we made a mask with narrow slits attached on the sputter head. In addition, we adjusted the slit shape to perform the coating uniformly in the vertical direction, which corresponds to the axial direction of the mirrors. We achieved the uniformity of $\pm 1\%$ over the range of 200 mm.

After the uniformity of the coating thickness was established, we carried out the platinum single-layer coating on the frontside and backside surfaces of the thin glass substrates. We found that the distortion by the frontside coating was at most ~ 1 μm even with a coating thickness of 320 Å. Furthermore, we demonstrated that the backside coating was successfully done to recover the surface profile of the glass substrates, indicating that the stress balancing worked well. We also performed the iridium single-layer coating on the both sides of the silicon mirrors. Because of the difference in the surface condition between the frontside and backside of the silicon mirrors, we found that only the same amount of the coatings cannot balance the residual stress for the silicon mirrors. However, the distortion was fully eliminated by an additional backside coating. It suggests that the stress balancing is also effective to the silicon mirrors, although the tuning of the amount of the backside coating should be required. We also applied our technique to the multilayer coating. However, the stress balancing by the single-layer backside coating did not fully remove the distortion for the Pt/C multilayer. The distribution of the residual stress induced by the multilayer should be examined to seek an appropriate method of the stress balancing.

REFERENCES

[1] Zhang, W. W. et al., "Next generation astronomical x-ray optics: high resolution, light weight, and low cost", *Astronomical Telescopes + Instrumentation 2018*, Proc. SPIE, in this conference.

[2] Riveros, R. E. et al., "Fabrication of lightweight silicon x-ray mirrors for high-resolution x-ray optics", *Astronomical Telescopes + Instrumentation 2018*, Proc. SPIE, in this conference.

[3] Civitani, M. M. et al., "Lynx optics based on full monolithic shells: design and development", *Astronomical Telescopes + Instrumentation 2018*, Proc. SPIE, in this conference.

[4] Reid, P. B. et al., "Development of adjustable x-ray optics for the Lynx mission concept", *Astronomical Telescopes + Instrumentation 2018*, Proc. SPIE, in this conference.

[5] Bavdaz, M. et al., "Development of the ATHENA mirror", *Astronomical Telescopes + Instrumentation 2018*, Proc. SPIE, in this conference.

[6] Collon, M. J. et al., "Silicon pore optics mirror module production and testing", *Astronomical Telescopes + Instrumentation 2018*, Proc. SPIE, in this conference.

[7] Chan, K.-W. et al., "Reflective coating for lightweight x-ray optics", *Space Telescopes + Instrumentation 2012*, Proc. SPIE, 8443, 84433S (2012).

[8] Chan, K.-W. et al., "Coating thin mirror segments for lightweight x-ray optics", *Optics for EUV, X-Ray, and Gamma-Ray Astronomy VI*, Proc. SPIE, 8861, 88610X (2013).

[9] Awaki, H., Kunieda, H., Ishida, M., et al., "Hard x-ray telescopes to be onboard ASTRO-H", Applied Optics, 53, 7664 (2014)

[10] Tamura, K., Kunieda, H., Miyata, Y., et al., "Supermirror design for Hard X-Ray Telescopes on-board Hitomi (ASTRO-H)", Journal of Astronomical Telescopes, Instruments, and Systems, 4, 01120 (2018)